

Intensive and broad bound exciton emission at cryogenic temperature in suspended monolayer transition metal dichalcogenides

Yunkun Wang (王云坤),¹ Yongzhi Xie (谢永志),¹ Yunyun Dai (戴贇贇),² Xu Han (韩旭),²
Yuan Huang (黄元) ^{2,*} and Yunan Gao (高宇南) ^{1,3,4,5,†}

¹State Key Laboratory for Artificial Microstructure and Mesoscopic Physics, School of Physics, Peking University, Beijing 100871, People's Republic of China

²Advanced Research Institute of Multidisciplinary Science, Beijing Institute of Technology, Beijing 100081, People's Republic of China

³Frontiers Science Center for Nano-Optoelectronics, Beijing 100871, People's Republic of China

⁴Collaborative Innovation Center of Extreme Optics, Shanxi University, Taiyuan 030006, People's Republic of China

⁵Peking University Yangtze Delta Institute of Optoelectronics, Nantong, Jiangsu 226010, People's Republic of China



(Received 5 June 2022; revised 30 September 2022; accepted 7 October 2022; published 4 November 2022)

Two-dimensional (2D) transition metal chalcogenides (TMDCs) are expected to play an important role in next-generation optoelectronic devices. However, the properties of 2D TMDCs can be largely affected by defects, and thus, many efforts have been made to characterize and eliminate the defects. Here, we investigate defect-related trap states, particularly in large-area suspended WS₂ monolayers at cryogenic temperatures, using steady-state and time-resolved photoluminescence (TRPL) spectroscopy. We observed an intensive and broad (full width half maximum \sim 170 meV) photoluminescence (PL) emission centered at 1.83 eV, 0.3 eV lower than the free exciton transition energy. From temperature-dependent PL spectra, the thermal activation energy of excitons escaping from trap states is determined to be 30 meV. The TRPL spectrum shows an ultralong lifetime at 13 K. The long-lived emission with the broad PL linewidth is attributed to excitons bound to defects of possibly chalcogenide-site substitution and sulfur vacancies. Compared with the supported monolayer, the defect-related trap states are found to be deeper in the suspended layer and can trap excitons more efficiently due to less dielectric screening. In this letter, we provide further understanding of trap states and decay channels in monolayer TMDCs and show that suspended 2D TMDCs can provide a pure platform for studying defect-related properties.

DOI: [10.1103/PhysRevMaterials.6.L111001](https://doi.org/10.1103/PhysRevMaterials.6.L111001)

I. INTRODUCTION

Two-dimensional (2D) transition metal dichalcogenides (TMDCs) have attracted great interest in both fundamental physics and promising applications due to their excellent properties such as high carrier mobility [1–3] and optical controllable valley polarization [4,5]. These properties make 2D TMDCs promising materials for compact functional devices such as transistors, photodetectors, valleytronic devices, and spintronic devices [2,3,6–11]. Defects in 2D TMDCs have been found to severely impact the performance of these devices [12]. Point defects such as vacancies and atomic substitution produce midgap defect states, which can efficiently trap free carriers. Excitons trapped at these defect sites will form bound excitons (BXs). If radiative recombination is possible, the BX will emit light at energies lower than the transition energy of free excitons. This phenomenon has been frequently observed in TMDCs such as MoS₂, WS₂, WSe₂, and MoSe₂ [13–29].

Numerous efforts have been made to correlate the defect structures with the corresponding photoluminescence (PL)

properties. For monolayer WS₂, Carozo *et al.* [17] showed that monosulfur vacancies (V_S) lead to two BX transitions X^{B1} and X^{B2} and the X^{B1} (X^{B2}) emission peak is \sim 30 meV (\sim 300 meV) below the free exciton emission. More recently, using scanning tunneling microscopy, Schuler *et al.* [30] found that the large splitting of \sim 250 meV of these two defect states is caused by spin-orbit coupling. They further demonstrated that chromium substitution of tungsten (Cr_W) also produces broad midgap defect states [31], whereas oxygen substitution of chalcogen site (O_S) and molybdenum substitution tungsten (Mo_W) do not [32]. For other TMDCs, the recombination of BXs has been attributed to excitons bound to ionized donors, impurity, doped atoms, and adsorbates [22,28,29,33]. Overall, the exact atomic origin of BXs emission is still not fully understood [12].

2D materials are highly sensitive to substrates, interfaces, and surrounding environments. Suspended 2D materials can avoid the substrate-induced effects and thus would be ideal for studying their intrinsic properties [34–36]. It is reported that PL efficiency is improved in suspended sample because the doping effect from substrate is avoided [34]. Although the PL of some suspended 2D materials at room temperature has been examined, the PL properties of suspended 2D materials at cryogenic temperatures are yet to be studied.

*yhuang@bit.edu.cn

†gyn@pku.edu.cn

In this letter, we investigate BXs in the suspended monolayer WS_2 at cryogenic temperatures by using steady-state and time-resolved PL (TRPL) spectroscopy. At 13 K, we observed an intensive emission centered at 1.83 eV, 0.3 eV lower than the free exciton transition energy, and extending >300 meV. This broad emission has an ultralong lifetime. From the PL spectroscopy results and further scanning transmission electron microscopy (STEM) measurement, we attributed this broad emission to excitons bound to defects of chalcogenide-site substitutes and sulfur vacancies. Compared with the region on the substrate, we found that the BX emission in the suspended TMDCs is more prominent than that in the region supported by the SiO_2/Si substrate because of weaker dielectric screening at the suspended area, resulting in the deeper energy level of defect states.

II. METHOD

A. Preparation of suspended 2D materials

The chemical-vapor-transport-grown bulk crystals of WS_2 were bought from 2D Semiconductors. To prepare the suspended sample, firstly, the SiO_2/Si substrate with the hole array was patterned by optical lithography and plasma etching. To avoid optical interference and gas pressure-induced strain in the PL measurement, the holes were completely etched through. After that, a thin layer of metal (Au/Ti: 5 nm/2 nm) was deposited onto the substrate with hole array. Then a new surface of layered crystal was cleaved by tape and put onto the substrate surface. A large area of suspended 2D materials can be exfoliated onto the hole-array substrate.

B. Steady-state PL measurements

The samples were cooled down to liquid helium temperature by MicrostatHires2 (Oxford Instruments). A continuous 532 nm laser was used to excite the samples. The laser spot was focused to $1 \mu\text{m}$ in diameter by an objective lens ($40\times$, numerical aperture = 0.6). The reflected PL signals were collected by the same lens, filtered by a 593 nm long pass filter. The PL spectra were analyzed by a spectrometer (Kymera 328i, Andor).

C. TRPL measurements

TRPL were collected by a streak camera (Hamamatsu C5680-04). The samples were excited at 558 nm by using an optical parametric oscillator pumped by Ti:sapphire oscillator. The repetition frequency of the femtosecond laser was 76 MHz, corresponding to a 13 ns pulse interval. The laser spot was $\sim 1 \mu\text{m}$ in diameter. PL signals were filtered by a 593 nm long pass filter to separate the emission of the sample from the excitation light.

III. RESULTS AND DISCUSSION

Millimeter-scale suspended monolayer WS_2 was exfoliated onto the hole-array substrate, using the gold-film-assisted exfoliation method reported recently [37,38], as illustrated in Fig. 1(a). The optical image of exfoliated monolayer WS_2 on the hole-array SiO_2/Si is shown in Fig. 1(b). The monolayer regions are marked with white dashed lines. Figure 1(c)

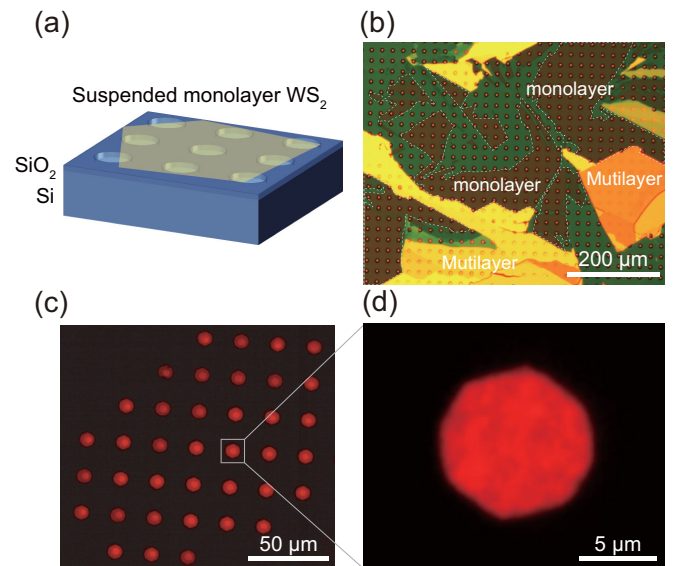


FIG. 1. The fabrication and image of large area suspended monolayer WS_2 . (a) Illustration of suspended monolayer WS_2 on prepatterned SiO_2/Si substrate. (b) Optical image of exfoliated monolayer WS_2 on the hole-array substrate. The monolayer regions are marked with the white dashed lines. The bright yellow flakes are multilayer regions. (c) Photoluminescence (PL) image of large area suspended monolayer WS_2 . (d) PL image of magnified monolayer suspended region.

presents the PL image of the monolayer region obtained at room temperature. The suspended regions show bright PL, while the supported area is dark because the gold beneath the monolayer quenches the PL [39]. Figure 1(d) shows a magnified PL image of a WS_2 monolayer on a single hole with a diameter of $10 \mu\text{m}$, where uniform brightness can be seen.

We first measured the steady-state PL of the suspended monolayer WS_2 at cryogenic temperatures. A 532 nm continuous laser was focused to a spot with the diameter of $\sim 1 \mu\text{m}$ in the center of the hole to excite the sample. Figure 2(a) shows the excitation power-dependent PL spectrum at 13 K, where the broad PL emission centered at 1.83 eV (full width at half maximum ~ 170 meV) is the most prominent feature. This emission peak is ~ 0.3 eV below the free exciton energy, and its width extends >300 meV. With the increase of excitation power, this broad emission grows much slower than free excitons, as shown in Fig. 2(a). Based on its lower energy and saturation behavior, we attribute the broad emission to the BX emission. Similar broad emission in monolayer WS_2 at low temperature has been reported to be due to free excitons bound to midgap states introduced by various sources [16,22,40]. The assignment of PL peaks at 2.087 eV to neutral excitons (X), 2.062 eV to negative trions (X^-) and 2.041 eV to biexciton complexes (charge neutral biexciton XX or negative charged biexciton XX^-) is based on the literature, and a detailed discussion is included in Supplemental Material Sec. 1 [41] (see also Refs. [42–46] therein).

The power law dependence of the PL intensity as a function of excitation power for BXs and free excitons is shown in Fig. 2(b). The PL intensity of a BX is integrated between the

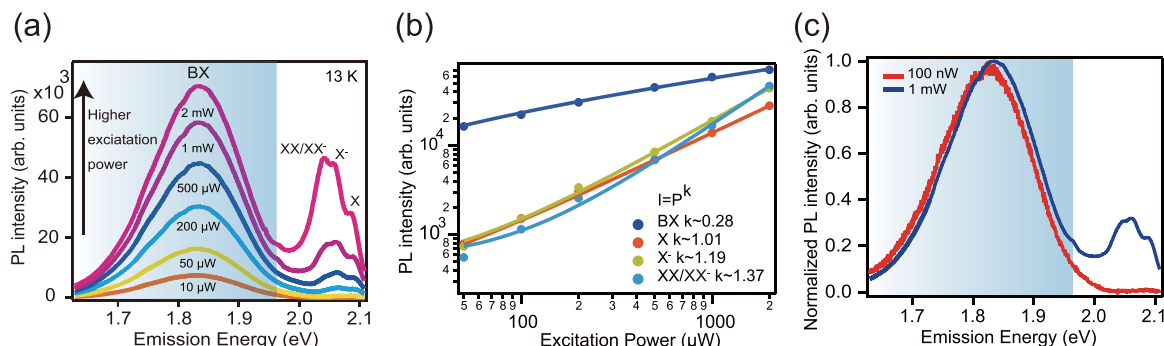


FIG. 2. Excitation power-dependent photoluminescence (PL) of suspended monolayer WS₂ acquired at 13 K. (a) Power-dependent PL of suspended monolayer WS₂. (b) Power law fitting of emission peaks. The bound exciton (BX) shows sublinear power dependence with $k \sim 0.28$. (c) Comparison of normalized PL intensity at 100 nW and 1 mW excitation power. A 12 meV blueshift of BX can be observed.

photon energies of 1.97 and 1.63 eV, and the intensities of various free exciton species are extracted by fitting using a multi-Gaussian function. The relation between PL intensity I and excitation power P is fitted by $I \sim P^k$. The BXs exhibit a sublinear power law dependence with k of 0.28 because the defect states are finite and get saturated at higher laser powers. The k of X, X⁻, and XX/XX⁻ are 1.01, 1.19, and 1.37, respectively, for which linear and superlinear dependencies are in good agreement with other reported studies [45,47–49].

As shown in Fig. 2(c), as the excitation power increases, the emission spectrum shifts to higher energies with little change in the line shape. When the excitation power was increased from 100 nW to 1 mW, the blueshift reached 12 meV. We interpret that this blueshift is due to the state-filling effect of BX states, as higher energy levels of defect states are filled with more photogenerated excitons. Eventually, the emission of free excitons becomes stronger with the gradual filling of defect states, as shown in Fig. 2(a). The spectral shift caused by the state filling effect can be well modeled by the Fermi-Dirac distribution for six orders of excitation powers, as shown in Fig. S2 in the Supplemental Material [41]. This interpretation is further supported by a temperature-dependent spectral line shape analysis, that is, at higher temperature, the Fermi-Dirac distribution curve becomes broader, as shown in Fig. S3 in the Supplemental Material [41].

Figure 3(a) shows PL spectra of BXs at an excitation power of 100 μW at different temperatures. The PL intensity of

BXs decreases with temperature increasing. The temperature dependence of the PL intensity (normalized to the value at 13 K) is shown in Fig. 3(b). When the temperature rises to 100 K, the emission of BXs almost loses its intensity. At room temperature, it becomes almost absent [see Fig. S4 in the Supplemental Material [41]]. The trend toward lower PL intensity for BXs at higher temperatures suggests thermal activated escape of these BXs from the midgap trap states.

The normalized BX PL intensity I as a function of temperature T can be modeled by the Arrhenius equation [50]:

$$I(T) = \frac{1}{1 + (k_A/k_R)\exp(-E_A/k_B T)}, \quad (1)$$

where k_B is the Boltzmann constant, E_A is the activation energy, k_A describes the thermal dissociation rate, k_R is the radiative emission rate of a BX, and E_A is determined to be ~ 30 meV between the excitation powers from 100 nW to 100 μW. The relative rate of k_A/k_R is >500 [Fig. S5 in the Supplemental Material [41]], indicating the thermal dissociation rate is much higher than the radiative emission rate of a BX. We use numerical simulation to show the robustness in extracting the value of E_A and k_A/k_R from Eq. (1), as presented in Supplemental Material Sec. 5 [41]. In the TRPL measurements presented later, the radiative emissivity is indeed found to be very low. The large k_A/k_R of BXs means that dissociation is more likely than radiative

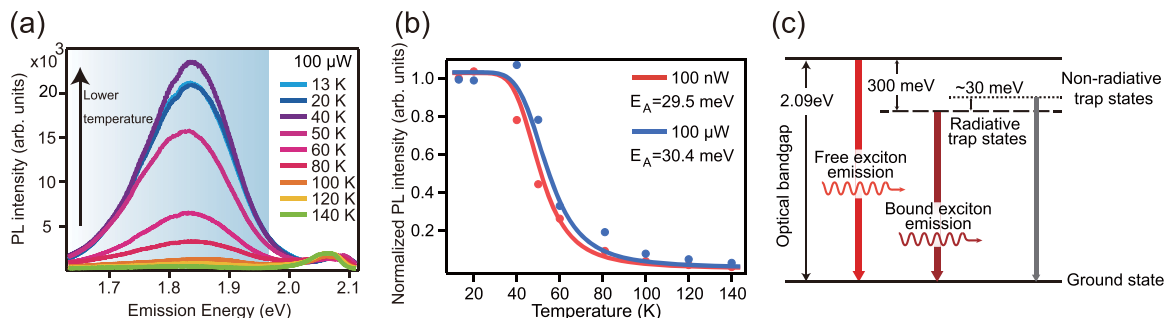


FIG. 3. Temperature-dependent photoluminescence (PL) of suspended monolayer WS₂. (a) The temperature-dependent PL spectra of suspended monolayer WS₂ acquired at 100 μW excitation power. (b) The temperature dependence of the normalized PL intensities of bound exciton intensity at 100 nW and 100 μW excitation powers (dots), and the Arrhenius equation fitting (lines). (c) Illustration of states and decay process.

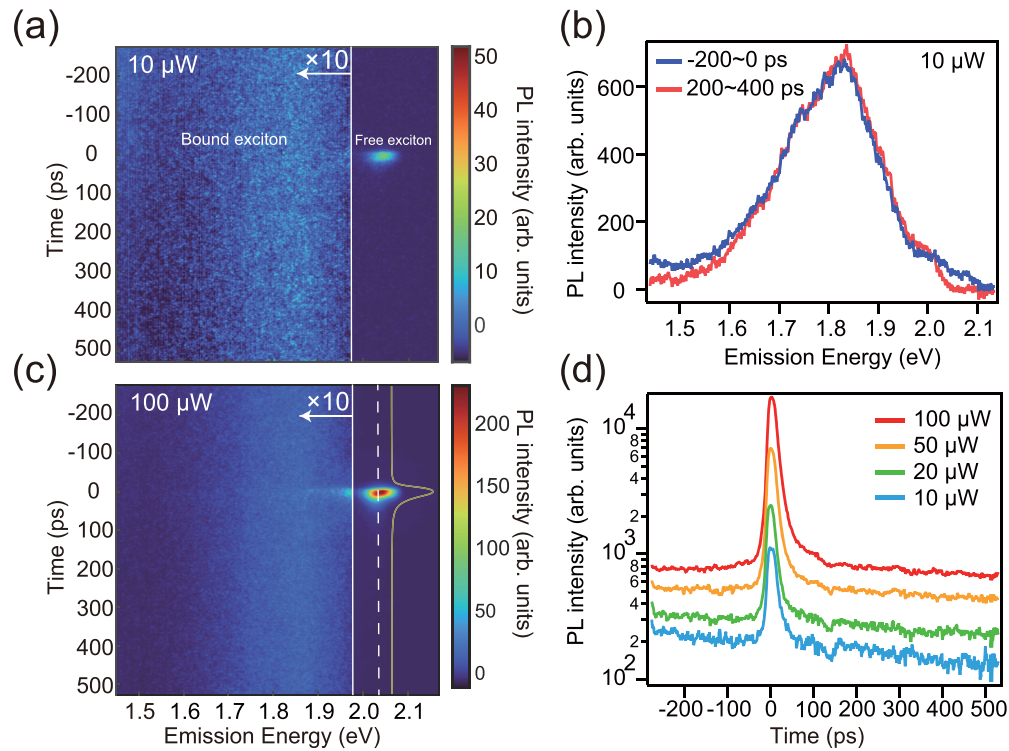


FIG. 4. Time-resolved photoluminescence (PL) spectroscopy of suspended monolayer WS_2 at 13 K. (a) At $10 \mu\text{W}$ excitation power, the bound exciton (BX) emission is nearly static with a long-lived component, and the contribution from the free exciton is also noticeable. (b) The integrated PL intensity of a BX between -200 and 0 ps (at the end of one pulse period, the time interval is 13.2 ns), and the intensity integrated between 200 and 400 ps (at the beginning of one pulse period). (c) At $100 \mu\text{W}$ excitation power, the intensity of BX emission still maintains with time decay, while the free excitons decay fast and take a larger proportion. The overlaid curve shows the dynamics of free excitons. (d) The excitation power-dependent decay dynamics of overall PL emission in logarithmic intensity coordinates.

recombination, which explains the rapid PL quenching with increasing temperature.

The thermal activation energy of these BXs (~ 30 meV) is found to be quite low, well below the 300 meV energy difference between the free exciton and BX peaks. Considering the relatively low PL quantum yield of typical WS_2 monolayers at both room temperature and low temperature, we infer that some dark states, in which the excitons decay nonradiatively, may exist above the BX states. Figure 2(a) shows that the decrease of the BX PL intensity with the increase of temperature is much larger than the increase in PL intensity of the free exciton, indicating that only a small fraction of BXs is converted to free excitons. A schematic diagram of the energy states and associated processes is shown in Fig. 3(c).

To further study the decay dynamics of the BXs, we measured the TRPL at 13 K using a streak camera. The sample was excited by a 76 MHz pulsed laser at 558 nm (2.22 eV) with a spot size of $\sim 1 \mu\text{m}$. As shown in Figs. 4(a) and 4(c), the BXs have remarkable long-lived emission. The repetition rate of 76 MHz corresponds to a 13.2 ns pulse interval. During the time between adjacent pulses, the BX emission is nearly static. As shown in Fig. 4(b), the PL intensity of BX integrated between -200 and 0 ps (at the end of one pulse period) is almost the same as the intensity integrated between 200 and 400 ps (at the beginning of one pulse period), which indicates a very long lifetime, i.e., a small emission rate, of these BXs.

Due to the time window limitation of our streak camera, the lifetime of BXs cannot be extracted accurately in this experiment. The PL lifetime of a BX is determined to be $\sim 1.5 \mu\text{s}$ by using a single photon detector, as shown in Figs. S7 and S8 in the Supplemental Material [41]. The long lifetime of BXs is in good agreement with the relatively large k_A/k_R determined from the temperature-dependent steady-state PL spectra shown in Fig. 3.

At a higher excitation $100 \mu\text{W}$, the BX emission still largely retains its long lifetime, while the PL from free excitons becomes more pronounced, as shown in Fig. 4(c). The overall intensity decay dynamics in relation to excitation power are shown in Fig. 4(d), where BXs contribute a flat basis in the decay curve, while free excitons account for a fraction of the fast decay with a short lifetime of ~ 20 ps. With increasing excitation power, the fraction of fast channels grows much faster than the basis, illustrating the saturation behavior of BXs, consistent with the steady-state PL shown in Fig. 2(b).

Combined with steady-state and TRPL results at different excitation intensities and temperatures, the behavior of the observed BX emission can be well understood. At low temperatures, most of the free excitons are trapped at defect sites, forming BXs that radiatively decay to the ground state at a very slow rate, while a small fraction of free excitons radiatively recombine at a faster rate before being trapped, as shown in Figs. 4(a) and 2(a). At increased temperatures,

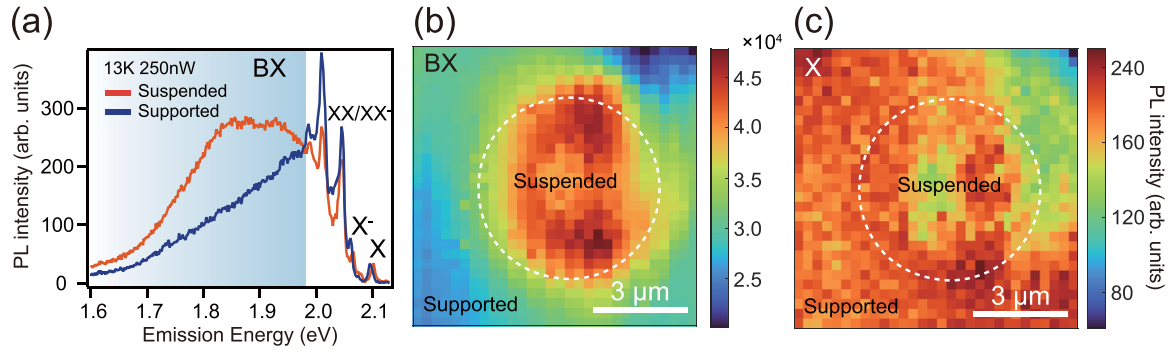


FIG. 5. Substrate effect on the bound exciton (BX) emission. (a) Comparison of photoluminescence (PL) spectrum from suspended and SiO_2/Si supported monolayer WS_2 , acquired at 13 K and 250 nW excitation power. (b) and (c) PL spatial mapping of BX and neutral exciton (X) obtained by integrating the PL spectrum from 1.50 to 1.98 eV and 2.08 to 2.11 eV, respectively. The suspended area is circled by white dotted line.

thermal energy helps long-lived BXs reach nonradiative trap states. Therefore, the emission of BXs is effectively quenched (Fig. 3). At room temperature, the BXs cannot form, and no emission can be observed.

Furthermore, we investigate the effect of the surrounding dielectric environment on the emission of BXs. A monolayer WS_2 on a hole-patterned SiO_2/Si substrate (without gold deposition) was made using the polydimethylsiloxane-based transfer method. The PL spectra of suspended and SiO_2/Si -supported monolayer WS_2 were obtained at 13 K and 250 nW excitation power, as shown in Fig. 5(a). The BX emission intensity (integrated from 1.50 to 1.98 eV) of the suspended region is approximately twice that of the supported region [see Fig. 5(b)], and the free exciton emission intensity (integrated from 2.08 to 2.11 eV) of the two regions is almost equal [see Fig. 5(c)]. The suspended area is circled by the white dotted line.

The density of defect states is independent of the underlying substrate, whereas the energy distribution of defect-related bound emission may be strongly dependent. It has been reported that the trap state distribution is monotonically related to the dielectric constant of the substrate [51]. The suspended environment has the lowest permittivity, resulting in deeper trap states and exhibiting more intensive BX emission. It is reported that the doping effect can play an important role in the recombination from charged defect states [22]. However, we find the doping does not play a major role here since the area ratio of excitons and trions (X/X^-) is almost the same at suspended and supported areas, as shown in Fig. S9 in the Supplemental Material [41].

Lastly, we note that the broad-BX emission feature cannot be eliminated by multiple heating and cooling cycles in vacuum, annealing in a 10% $\text{H}_2/90\%$ Ar mixture at 450 K, and laser irradiation. These observations suggest that the broad peak is less likely to be due to external absorbers but more likely to be due to natural defects in the WS_2 crystals. We did observe some point defects in our sample using STEM, as shown in Fig. S10 in the Supplemental Material

[41], possibly chromium substituting tungsten and sulfur vacancy. It is reported that these two kinds of defects result in a midgap trap state [30,31,52]. Since there could be trace elements like Cr present in the WO_3 and MoO_3 precursor, they may participate in the reaction of synthesizing the bulk and few-layer materials. However, due to the relatively low sensitivity of the x-ray photoelectron spectroscopy (XPS) technique, no signal of Cr was detected in XPS measurement, as discussed in Fig. S11 in the Supplemental Material [41].

IV. CONCLUSIONS

In summary, we observed an intensive and broad BX emission in suspended WS_2 monolayers at cryogenic temperatures. Its intensity exhibits a saturation behavior with increasing excitation power and fades away with increasing of temperature. The TRPL spectra show the BX emission has an ultralong lifetime. Its origin is attributed to excitons bound to defects of chalcogenide-site substitutes and sulfur vacancies. In supported monolayers, due to dielectric screening of the substrate, the BX emission is weaker. In this letter, we provide further understanding of defect states and decay channels in suspended TMDCs and show that suspended 2D TMDCs can be a pure platform for studying defect-related properties.

ACKNOWLEDGMENTS

This letter is supported by the National Key Research and Development Program of China (Grants No. 2018YFA0306302 and No. 2019YFA0308000), the National Natural Science Foundation of China (Grants No. 61875002, No. 62022089, No. 11874405, and No. 52272135), the Strategic Priority Research Program (B) of the Chinese Academy of Sciences (Grant No. XDB33000000), and Chongqing Outstanding Youth Fund (Grant No. 2021ZX0400005).

The authors declare no conflict of interest.

- [1] C. Chang, W. Chen, Y. Chen, Y. Chen, Y. Chen, F. Ding, C. Fan, H. J. Fan, Z. Fan, and C. Gong, Recent progress on two-dimensional materials, *Acta Phys.-Chim. Sin.* **37**, 2108017 (2021).
- [2] B. Radisavljevic, A. Radenovic, J. Brivio, V. Giacometti, and A. Kis, Single-layer MoS₂ transistors, *Nat. Nanotechnol.* **6**, 147 (2011).
- [3] B. Radisavljevic and A. Kis, Mobility engineering and a metal-insulator transition in monolayer MoS₂, *Nat. Mater.* **12**, 815 (2013).
- [4] K. F. Mak, K. He, J. Shan, and T. F. Heinz, Control of valley polarization in monolayer MoS₂ by optical helicity, *Nat. Nanotechnol.* **7**, 494 (2012).
- [5] T. Cao, G. Wang, W. Han, H. Ye, C. Zhu, J. Shi, Q. Niu, P. Tan, E. Wang, B. Liu *et al.*, Valley-selective circular dichroism of monolayer molybdenum disulfide, *Nat. Commun.* **3**, 887 (2012).
- [6] Y. Q. Bie, G. Grosso, M. Heuck, M. M. Furchi, Y. Cao, J. Zheng, D. Bunandar, E. Navarro-Moratalla, L. Zhou, D. K. Efetov *et al.*, A MoTe₂-based light-emitting diode and photodetector for silicon photonic integrated circuits, *Nat. Nanotechnol.* **12**, 1124 (2017).
- [7] Y. Xie, B. Zhang, S. Wang, D. Wang, A. Wang, Z. Wang, H. Yu, H. Zhang, Y. Chen, M. Zhao *et al.*, Ultrabroadband MoS₂ photodetector with spectral response from 445 to 2717 nm, *Adv. Mater.* **29**, 1605972 (2017).
- [8] O. L. Sanchez, D. Ovchinnikov, S. Misra, A. Allain, and A. Kis, Valley polarization by spin injection in a light-emitting van der Waals heterojunction, *Nano Lett.* **16**, 5792 (2016).
- [9] Y. J. Zhang, T. Oka, R. Suzuki, J. T. Ye, and Y. Iwasa, Electrically switchable chiral light-emitting transistor, *Science* **344**, 725 (2014).
- [10] Y. Liu and Q. Shao, Two-dimensional materials for energy-efficient spin-orbit torque devices, *ACS Nano* **14**, 9389 (2020).
- [11] A. Avsar, H. Ochoa, F. Guinea, B. Özyilmaz, B. J. van Wees, and I. J. Vera-Marun, Colloquium: Spintronics in graphene and other two-dimensional materials, *Rev. Mod. Phys.* **92**, 021003 (2020).
- [12] M. Zhou, W. Wang, J. Lu, and Z. Ni, How defects influence the photoluminescence of TMDCs, *Nano Res.* **14**, 29 (2021).
- [13] T. Yan, X. Qiao, X. Liu, P. Tan, and X. Zhang, Photoluminescence properties and exciton dynamics in monolayer WSe₂, *Appl. Phys. Lett.* **105**, 101901 (2014).
- [14] J. Jadczyk, J. Kutrowska-Girzycka, P. Kapuscinski, Y. S. Huang, A. Wojs, and L. Bryja, Probing of free and localized excitons and trions in atomically thin WSe₂, WS₂, MoSe₂ and MoS₂ in photoluminescence and reflectivity experiments, *Nanotechnology* **28**, 395702 (2017).
- [15] S. Zhang, C. G. Wang, M. Y. Li, D. Huang, L. J. Li, W. Ji, and S. Wu, Defect Structure of Localized Excitons in a WSe₂ Monolayer, *Phys. Rev. Lett.* **119**, 046101 (2017).
- [16] T. Kato and T. Kaneko, Optical detection of a highly localized impurity state in monolayer tungsten disulfide, *ACS Nano* **8**, 12777 (2014).
- [17] V. Carozo, Y. Wang, K. Fujisawa, B. R. Carvalho, A. McCreary, S. Feng, Z. Lin, C. Zhou, N. Perea-López, and A. L. Elías, Optical identification of sulfur vacancies: bound excitons at the edges of monolayer tungsten disulfide, *Sci. Adv.* **3**, e1602813 (2017).
- [18] Y. Lee, S. J. Yun, Y. Kim, M. S. Kim, G. H. Han, A. K. Sood, and J. Kim, Near-field spectral mapping of individual exciton complexes of monolayer WS₂ correlated with local defects and charge population, *Nanoscale* **9**, 2272 (2017).
- [19] M. R. Molas, K. Nogajewski, A. O. Slobodeniuk, J. Binder, M. Bartos, and M. Potemski, The optical response of monolayer, few-layer and bulk tungsten disulfide, *Nanoscale* **9**, 13128 (2017).
- [20] J. Shang, C. Cong, X. Shen, W. Yang, C. Zou, N. Peimyoo, B. Cao, M. Eginligil, W. Lin, W. Huang *et al.*, Revealing electronic nature of broad bound exciton bands in two-dimensional semiconducting WS₂ and MoS₂, *Phys. Rev. Mater.* **1**, 074001 (2017).
- [21] V. Orsi Gordo, M. A. G. Balanta, Y. Galvao Gobato, F. S. Covre, H. V. A. Galeti, F. Iikawa, O. D. D. Couto, F. Qu, M. Henini, D. W. Hewak *et al.*, Revealing the nature of low-temperature photoluminescence peaks by laser treatment in van der Waals epitaxially grown WS₂ monolayers, *Nanoscale* **10**, 4807 (2018).
- [22] K. Greben, S. Arora, M. G. Harats, and K. I. Bolotin, Intrinsic and extrinsic defect-related excitons in TMDCs, *Nano Lett.* **20**, 2544 (2020).
- [23] R. Kaupmees, M. Grossberg, M. Ney, A. Asaithambi, A. Lorke, and J. Krustok, Tailoring of bound exciton photoluminescence emission in WS₂ monolayers, *Phys. Status Solidi RRL* **14**, 1900355 (2020).
- [24] R. Kumar, I. Verzhbitskiy, and G. Eda, Strong optical absorption and photocarrier relaxation in 2-D semiconductors, *IEEE J. Quantum Electron.* **51**, 1 (2015).
- [25] A. J. Goodman, A. P. Willard, and W. A. Tisdale, Exciton trapping is responsible for the long apparent lifetime in acid-treated MoS₂, *Phys. Rev. B* **96**, 121404(R) (2017).
- [26] J. Wierzbowski, J. Klein, F. Sigger, C. Straubinger, M. Kremser, T. Taniguchi, K. Watanabe, U. Wurstbauer, A. W. Holleitner, M. Kaniber *et al.*, Direct exciton emission from atomically thin transition metal dichalcogenide heterostructures near the lifetime limit, *Sci. Rep.* **7**, 12383 (2017).
- [27] Y. Yu, J. Dang, C. Qian, S. Sun, K. Peng, X. Xie, S. Wu, F. Song, J. Yang, S. Xiao *et al.*, Many-body effect of mesoscopic localized states in MoS₂ monolayer, *Phys. Rev. Mater.* **3**, 051001(R) (2019).
- [28] E. Mitterreiter, B. Schuler, A. Micevic, D. Hernangómez-Pérez, K. Barthelmi, K. A. Cochrane, J. Kiemle, F. Sigger, J. Klein, E. Wong *et al.*, The role of chalcogen vacancies for atomic defect emission in MoS₂, *Nat. Commun.* **12**, 3822 (2021).
- [29] T. Venanzi, H. Arora, A. Erbe, A. Pashkin, S. Winnerl, M. Helm, and H. Schneider, Exciton localization in MoSe₂ monolayers induced by adsorbed gas molecules, *Appl. Phys. Lett.* **114**, 172106 (2019).
- [30] B. Schuler, D. Y. Qiu, S. Refaely-Abramson, C. Kastl, C. T. Chen, S. Barja, R. J. Koch, D. F. Ogletree, S. Aloni, A. M. Schwartzberg *et al.*, Large Spin-Orbit Splitting of Deep In-Gap Defect States of Engineered Sulfur Vacancies in Monolayer WS₂, *Phys. Rev. Lett.* **123**, 076801 (2019).
- [31] B. Schuler, J. H. Lee, C. Kastl, K. A. Cochrane, C. T. Chen, S. Refaely-Abramson, S. Yuan, E. van Veen, R. Roldan, N. J. Borys *et al.*, How substitutional point defects in two-dimensional WS₂ induce charge localization, spin-orbit splitting, and strain, *ACS Nano* **13**, 10520 (2019).
- [32] S. Barja, S. Refaely-Abramson, B. Schuler, D. Y. Qiu, A. Pulkin, S. Wickenburg, H. Ryu, M. M. Ugeda, C. Kastl, C. Chen

- et al.*, Identifying substitutional oxygen as a prolific point defect in monolayer transition metal dichalcogenides, *Nat. Commun.* **10**, 3382 (2019).
- [33] F. Brandão, G. Ribeiro, P. Vaz, J. González, and K. Krambrock, Identification of rhenium donors and sulfur vacancy acceptors in layered MoS₂ bulk samples, *J. Appl. Phys.* **119**, 235701 (2016).
- [34] Y. Yu, Y. Yu, C. Xu, Y. Q. Cai, L. Su, Y. Zhang, Y. W. Zhang, K. Gundogdu, and L. Cao, Engineering substrate interactions for high luminescence efficiency of transition-metal dichalcogenide monolayers, *Adv. Funct. Mater.* **26**, 4733 (2016).
- [35] Y. Yu, Y. Yu, C. Xu, A. Barrette, K. Gundogdu, and L. Cao, Fundamental limits of exciton-exciton annihilation for light emission in transition metal dichalcogenide monolayers, *Phys. Rev. B* **93**, 201111(R) (2016).
- [36] Y. Sang, J. Guo, H. Chen, W. Yang, X. Chen, F. Liu, and X. Wang, Measurement of thermal conductivity of suspended and supported single-layer WS₂ using micro-photoluminescence spectroscopy, *J. Phys. Chem. C* **126**, 6637 (2022).
- [37] Y. Huang, Y.-H. Pan, R. Yang, L.-H. Bao, L. Meng, H.-L. Luo, Y.-Q. Cai, G.-D. Liu, W.-J. Zhao, Z. Zhou *et al.*, Universal mechanical exfoliation of large-area 2D crystals, *Nat. Commun.* **11**, 2453 (2020).
- [38] Y. Huang, Y. K. Wang, X. Y. Huang, G. H. Zhang, X. Han, Y. Yang, Y. Gao, L. Meng, Y. Wang, and G. Z. Geng, An efficient route to prepare suspended monolayer for feasible optical and electronic characterizations of two-dimensional materials, *InfoMat* **4**, e12274 (2022).
- [39] X. Huang, L. Zhang, L. Liu, Y. Qin, Q. Fu, Q. Wu, R. Yang, J.-P. Lv, Z. Ni, L. Liu *et al.*, Raman spectra evidence for the covalent-like quasi-bonding between exfoliated MoS₂ and Au films, *Sci. China. Inform. Sci.* **64**, 140406 (2021).
- [40] Z. He, X. Wang, W. Xu, Y. Zhou, Y. Sheng, Y. Rong, J. M. Smith, and J. H. Warner, Revealing defect-state photoluminescence in monolayer WS₂ by cryogenic laser processing, *ACS Nano* **10**, 5847 (2016).
- [41] See Supplemental Material at <http://link.aps.org/supplemental/10.1103/PhysRevMaterials.6.L111001> for additional details on assignment of free exciton components, PL line shape analysis of bound excitons, PL spectrum of monolayer WS₂ at room temperature, temperature-dependent PL intensity of bound excitons at different excitation power, numerical simulation of Arrhenius equation, power- and temperature-dependent TRPL of bound excitons, analysis of doping effect in our sample, and analysis on possible origin of bound exciton emission.
- [42] Y. Cho and T. C. Berkelbach, Environmentally sensitive theory of electronic and optical transitions in atomically thin semiconductors, *Phys. Rev. B* **97**, 041409 (2018).
- [43] Y. Kajino, K. Oto, and Y. Yamada, Modification of optical properties in monolayer WS₂ on dielectric substrates by coulomb engineering, *J. Phys. Chem. C* **123**, 14097 (2019).
- [44] S. Chatterjee, G. Gupta, S. Das, K. Watanabe, T. Taniguchi, and K. Majumdar, Trion-trion annihilation in monolayer WS₂, *Phys. Rev. B* **105**, L121409 (2022).
- [45] P. Nagler, M. V. Ballottin, A. A. Mitioglu, M. V. Durnev, T. Taniguchi, K. Watanabe, A. Chernikov, C. Schüller, M. M. Glazov, and P. C. Christianen, Zeeman Splitting and Inverted Polarization of Biexciton Emission in Monolayer WS₂, *Phys. Rev. Lett.* **121**, 057402 (2018).
- [46] G. Plechinger, P. Nagler, J. Kraus, N. Paradiso, C. Strunk, C. Schüller, and T. Korn, Identification of excitons, trions and biexcitons in single-layer WS₂, *Phys. Status Solidi (RRL)* **9**, 457 (2015).
- [47] G. Plechinger, P. Nagler, A. Arora, R. Schmidt, A. Chernikov, A. G. Del Águila, P. Christianen, R. Bratschitsch, C. Schüller, and T. Korn, Trion fine structure and coupled spin-valley dynamics in monolayer tungsten disulfide, *Nat. Commun.* **7**, 12715 (2016).
- [48] S. Chatterjee, S. Das, G. Gupta, K. Watanabe, T. Taniguchi, and K. Majumdar, Probing biexciton in monolayer WS₂ through controlled many-body interaction, *2D Mater.* **9**, 015023 (2021).
- [49] Z. Ye, L. Waldecker, E. Y. Ma, D. Rhodes, A. Antony, B. Kim, X.-X. Zhang, M. Deng, Y. Jiang, Z. Lu *et al.*, Efficient generation of neutral and charged biexcitons in encapsulated WSe₂ monolayers, *Nat. Commun.* **9**, 3718 (2018).
- [50] G. Bacher, H. Schweizer, J. Kovac, A. Forchel, H. Nickel, W. Schlapp, and R. Lösch, Influence of barrier height on carrier dynamics in strained In_xGa_{1-x}As/GaAs quantum wells, *Phys. Rev. B* **43**, 9312 (1991).
- [51] A. Goodman, D.-H. Lien, G. Ahn, L. Spiegel, M. Amani, A. Willard, A. Javey, and W. Tisdale, Substrate-dependent exciton diffusion and annihilation in chemically treated MoS₂ and WS₂, *J. Phys. Chem. C* **124**, 12175 (2020).
- [52] Y. Wan, E. Li, Z. Yu, J.-K. Huang, M.-Y. Li, A.-S. Chou, Y.-T. Lee, C.-J. Lee, H.-C. Hsu, Q. Zhan *et al.*, Low-defect-density WS₂ by hydroxide vapor phase deposition, *Nat. Commun.* **13**, 4149 (2022).